Sensors and Materials, Vol. 35, No. 10 (2023) 4527–4536
MYU Tokyo

Letter

S & M 3412

An Enhanced Performance of Glucose Biosensor Based on TiO_2 Nanorod Arrays Decorated with Ag Nanoparticles

Minghui Chen,[1,2] Jin Liu,[2] Pengzhao Chang,[1] Shaohui Zheng,[1] and Yong Wang[1*]

[1]School of Medical Imaging, Xuzhou Medical University, Xuzhou, Jiangsu 221004, China
[2]The Affiliated Hospital of Xuzhou Medical University, Xuzhou, Jiangsu 220005, China

(Received August 18, 2023; accepted September 28, 2023)

Keywords: TiO_2 NAs, Ag NPs, Ag NPs-TiO_2 NAs/CP electrode, glucose biosensor, sensitive glucose detection

In this study, TiO_2 nanorod arrays (NAs) on carbon paper (CP) substrates were prepared via hydrothermal synthesis. Then, Ag nanoparticles (NPs) were deposited on the surface of the TiO_2 NAs to enhance the electrocatalytic activity and analysis ability of the electrode for H_2O_2. Thereafter, GOx was modified on the surface of the Ag NPs-TiO_2 NAs/CP via the cross-linking method for the detection of glucose. The GOx/Ag NPs-TiO_2 NAs/CP integrates the functions of the specific recognition of glucose, signal transduction, and signal amplification. In an *in vitro* test, this GOx/Ag NPs-TiO_2 NAs/CP biosensor shows a sensitivity of 0.182 mA $mM^{-1}cm^{-2}$, which is 6.6-fold that for the GOx/CP sensor (0.0276 mA mM^{-1} cm^{-2}). The sensor can transduce the GOx-catalyzed reaction into significant current signals within 5 s. The relationship between the glucose concentration and the sensitivity to glucose is linear with the correlation coefficient R^2 of 0.9996 in the range of 0–0.9 mM, and the detection limit was estimated to be 1.6 μM.

1. Introduction

Diabetes mellitus is a worldwide public disease, which has seriously threatened human health over the long history of mankind.(1) Blood glucose monitoring is an important part of diabetes management. The results of blood glucose monitoring can reflect the degree of glucose metabolism disorder in diabetic patients, which can be used to develop reasonable hypoglycemic programs. Therefore, it is essential to develop a biosensor for the detection of blood glucose. The traditional glucose biosensor composed of glucose oxidase (GOx) electrodes is of critical significance for the detection of glucose concentration in the blood.(2) The GOx electrodes can be used to determine the blood glucose level by detecting the current generated by the enzyme redox reaction product H_2O_2 during the electrochemical reaction at the anode.(3) This enzyme-immobilized electrode biosensor has attracted considerable attention for the rapid detection of blood glucose *in vitro* owing to its advantages of simple structure, high sensitivity, excellent selectivity, and real-time glucose monitoring.

*Corresponding author: e-mail: wangyong@xzhmu.edu.cn
https://doi.org/10.18494/SAM4618

ISSN 0914-4935 © MYU K.K.
https://myukk.org/

Normally, the electrocatalytic activity of glucose biosensors is determined by various important factors, such as the composition of electrode materials, surface structure, and the immobilization of GOx on the electrode surface.[4] Nanostructured materials with a large specific surface area have exhibited many merits for the development of biosensors because they provide many active sites for the immobilization of GOx,[5,6] thus improving the immobilization efficiency of GOx and enhancing the electrocatalytic activity of the glucose sensor.[7] Therefore, various nanomaterials, such as C, Au, Pt, SiO_2, AlO_3, MnO_2, and TiO_2 nanoparticles, have been used to prepare GOx electrodes.

Among them, TiO_2 nanomaterials have shown many advantages in biosensor application, such as good biocompatibility, relatively high conductivity, nontoxicity, excellent stability, and low cost. Therefore, TiO_2 nanomaterials with various structures have been used to immobilize enzymes in the preparation of glucose electrode biosensors.[8,9] Compared with other nanostructures, highly ordered TiO_2 nanoarrays provide a one-way channel for electron transport and high electron conduction efficiency, and are widely used as carrier materials for GOx. For example, Wang *et al.* prepare GOx electrodes by grafting GOx on the surface of Ag NPs-deposited TiO_2 NAs, which showed high sensitivity for glucose detection.[10] However, owing to the effect of surface tension, the immobilized GOx and the diffused electrolyte solution cannot reach the interior area of the nanotube, hindering the catalytic efficiency of the glucose biosensor. Unlike TiO_2 nanotube arrays, TiO_2 NAs can facilitate the diffusion of the electrolyte solution to the bottom of the electrode without sacrificing the large specific surface area and high electron conduction efficiency, enabling them to be an ideal carrier material for the enzyme electrode.[11,12]

However, enzyme electrodes composed of pure TiO_2 nanomaterials usually exhibit low bio-electrocatalytic activity.[13] Noble metal nanoparticles, especially Pt, Au, and Ag nanoparticles, are often used in the preparation of composite nanomaterials owing to their high electrocatalytic activity, excellent conductivity, and large specific surface area.[14] These composites are often applied in surface-enhanced Raman scattering detection, photocatalysis, H_2O_2 biosensors, and glucose biosensors. Therefore, it is an effective approach to improve the electrocatalytic activity of electrode materials by coating the noble metal nanoparticles on the surface of TiO_2 nanomaterials.[15]

In addition, carbon paper (CP) is composed of carbon fiber skeleton and carbon material, which has the advantages of good electrical conductivity, stable property, and low price. CP also possesses a large specific surface owing to its rough surface and a large number of holes in its interior. This structural feature of CP enables it to be an ideal substrate for the growth of TiO_2 NAs. Herein, as shown in Fig. 1, we prepared TiO_2 NAs on the CP substrate via hydrothermal synthesis, then deposited Ag NPs on the surface of the TiO_2 NAs to enhance their electrocatalytic activity, and investigated the detection and analysis ability of the electrode for H_2O_2. We also modified the crosslinking method to immobilize GOx on the surface of the electrode to prepare the GOx/Ag NPs-TiO_2 NAs/CP electrode to observe the detection performance of the prepared electrode for glucose in the blood.

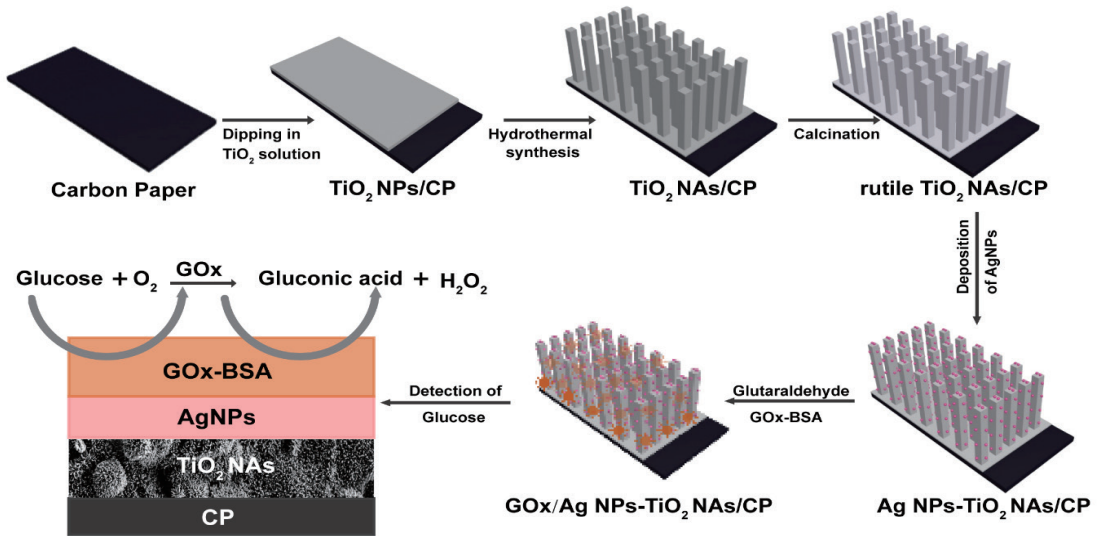

Fig. 1. (Color online) Schematic of synthesis of GOx/Ag NPs-TiO_2 NAs/CP and principle of glucose detection.

2. Materials and Methods

2.1 Materials

Butyl titanate, absolute ethanol, glacial acetic acid, hydrochloric acid, tetrabutyl titanate, polytetrafluoroethylene, ethanol, ethylene glycol, polyvinylpyrrolidone-k30 (PVP-k30), $NaBH_4$, $AgNO_3$, phosphate-buffered saline (PBS), and glutaraldehyde were purchased from Sigma-Aldrich (St. Louis, Missouri, USA). GOx, bovine serum albumin (BSA), and glucose were obtained from Solarbio Life Sciences (Beijing, China).

2.2 Preparation of AgNPs-TiO_2 Nas/CP electrode

2.2.1 Pretreatment of CP

The highly ordered Gox/AgNPs-TiO_2 Nas/CP electrodes were fabricated following the process shown in Fig. 1. Briefly, CP was first cut into small pieces of 50 × 20 × 0.20 mm^3 size, then each was sonicated for 10 min in acetone and deionized water, followed by drying at 80 °C for further use.

2.2.2 Preparation of TiO_2 solution

Butyl titanate (20 mL) was first added in a 200 mL beaker. Then, 100 mL of absolute ethanol was slowly added in the beaker with stirring. Thereafter, 0.2 ml of glacial acetic acid was also added dropwise to the above mixture. Finally, the reaction solution was stirred at room temperature until the mixture turned milky white.

2.2.3 Deposition of TiO_2 NPs on CP

The pretreated CPs were immersed in the TiO_2 solution for 5 min, dried at 80 °C, then heated on annealing at 350 °C for 20 min under vacuum conditions, and finally cooled to room temperature naturally.

2.2.4 Growth of TiO_2 NAs on CP via hydrothermal synthesis

Concentrated hydrochloric acid (18 mL, 36–38 wt%) was mixed with DI water (18 mL) and stirred for 5 min in a 50 mL beaker. Then, tetrabutyl titanate (0.54 mL) was added to the above mixture and stirred for 10 min. Thereafter, a polytetrafluoroethylene autoclave, in which TiO_2 NP-coated CPs and the resultant solution were sealed, was maintained at 180 °C for 10 h and cooled to room temperature to obtain CPs with a white layer formed at both sides. Finally, the samples were washed repeatedly to remove the residual reaction solution from the surface and dried.

2.2.5 Calcination treatment of TiO_2 NAs/CP

The dried samples of the TiO_2 NAs/CP were placed in an integrated programmable high-temperature furnace. The temperature was raised to 250 °C at a heating rate of 5 °C/min, maintained for 10 min, and raised to 500 °C at a heating rate of 5 °C/min, followed by calcination for 1.5 h at 500 °C. After the calcination, the amorphous NAs of TiO_2 NAs/CPs can be transformed into more orderly and regular rutile crystals.

2.2.6 Deposition of Ag NPs on TiO_2/CPs

DI water (15 mL) and ethylene glycol (15 mL) were mixed in a 50 mL beaker, followed by the addition of 1.2 g of PVP-k30 with stirring. Then, $NaBH_4$ (0.0296 g) was added to the above solution and stirred for 1–2 min, followed by the addition of $AgNO_3$ (0.1784 g) with stirring until the resultant solution became dark brown. Thereafter, the Ag NPs-TiO_2 NAs/CPs were immersed in the brown Ag solution at 40 °C for 10 h. Finally, the samples were washed carefully with DI water to obtain the Ag NPs-TiO_2 NAs/CP electrode.

2.3 Immobilization of GOx on Ag NPs-TiO_2 NAs/CP electrode

The GOx/Ag NPs-TiO_2 NAs/CP electrode was fabricated by immobilizing the GOx enzymes on the surface of the Ag NPs-TiO_2 NAs/CP electrode via the crosslinking of GOx and BSA. BSA was first fixed on the Ag NPs-TiO_2 NAs/CP electrode via deposition at 30 min, and GOx was conjugated to BSA through glutaraldehyde and then fixed on the outer surface of the Ag NPs-TiO_2 NAs/CP electrode. Briefly, BSA (25 mg) was first dispersed in PBS (1 mL, pH 6.8), followed by the addition of glutaraldehyde (100 μL), and then the above mixture was stored at 4 °C as a cross-linker. Then, the GOx solution was prepared by adding 2.5 mg of GOx in

PBS (0.1 mL, pH 6.8). Thereafter, the Ag NPs-TiO_2 NAs/CP electrode was immersed in PBS to wet the surface before GOx immobilization. Then, the Ag NPs-TiO_2 NAs/CP electrode was immobilized in the above BSA/glutaraldehyde mixture (20 μL/cm^2) and dried for 15 min at room temperature to allow the good adsorption of BSA on the Ag NPs-TiO_2 NAs/CP electrode. Subsequently, the GOx solution (20 μL) was coated on the above sample and stored for 12 h at 4 ℃ to immobilize GOx to the electrode. The prepared GOx/Ag NPs-TiO_2 NAs/CP electrode was immersed in PBS (pH 6.8) before use to remove free GOx molecules. GOx was also immobilized on CP and TiO_2 NAs-coated CP to fabricate the GOx-CP and GOx/TiO_2 NAs/CP electrode for comparison. All prepared GOx electrodes were stored at 4 ℃.

3. Results and Discussion

3.1 Characterization of GOx/Ag NPs-TiO_2 NAs/CP electrode

The GOx/Ag NPs-TiO_2 NAs/CP electrodes were characterized by field emission scanning electron microscopy (FE-SEM), transmission electron microscopy (TEM), X-ray diffraction (XRD), and energy-dispersive spectrometry (EDS) to investigate their structure and chemical composition. As shown in the photo of the electrode in Fig. 2(A), a uniform layer of TiO_2 can be observed on the surface of CPs after their immersion in a hydrothermal reaction solution of TiO_2. Figure 2(B) shows the nanoscale image of the TiO_2 NAs-coated CP electrode. As shown in Fig. 2(C), both the top surface of the CP and internal holes in the CP were uniformly covered with the TiO_2 NAs, indicating the excellent hydrothermal growth of the TiO_2 NAs on the CPs. In addition, as indicated in Fig. 2(D), the TiO_2 nanorods (NRs) were observed to have a quadrangular morphology with a smooth and flat surface and a rod thickness of approximately 100 nm. Moreover, TiO_2 NRs presented an average height of about 1.5 μm from Fig. 2(D). Previously, the fluorine-doped tin oxide (FTO) conducting glass was conventionally applied as the substrate for the growth of TiO_2 NAs. However, compared with the FTO conducting glass, CPs demonstrated the advantages of stable chemical property, low price, and so forth. Furthermore, the porous structure of CP can provide a much larger surface area for the growth of TiO_2 NAs to load more electrodes on CP.

The TiO_2 NA-coated CPs were also investigated by EDS. As shown in Fig. 2(E), the EDS spectrum for the TiO_2 NAs-coated CPs exhibited the peak due to the elements C, O, and Ti. The results also demonstrated the successful coating of TiO_2 NAs on the CPs. Prior to the observations of the morphologies of TiO_2 NAs, the TiO_2 NAs/CPs were ultrasonicated in ethanol to peel the TiO_2 NRs from the CPs. Then, the TiO_2 NR suspension was loaded on a copper grid and observed by TEM and simulation electron diffraction (SAED). As indicated in Figs. 2(F) and 2G, the TiO_2 NRs presented a uniform column morphology with a thickness of 70–100 nm and excellent crystallinity. In addition, Fig. 2(H) shows the XRD pattern of the TiO_2 NAs/CP, standard card of rutile TiO_2 (JCPDs Card No. 21-1276) and the standard card of carbon (JCPDs Card No. 26-1076). It was observed that the diffraction peaks of TiO_2 NRs were consistent with the standard card of rutile TiO_2, and there was no clear miscellaneous peak, indicating that the prepared TiO_2 nanorod was a rutile crystal.

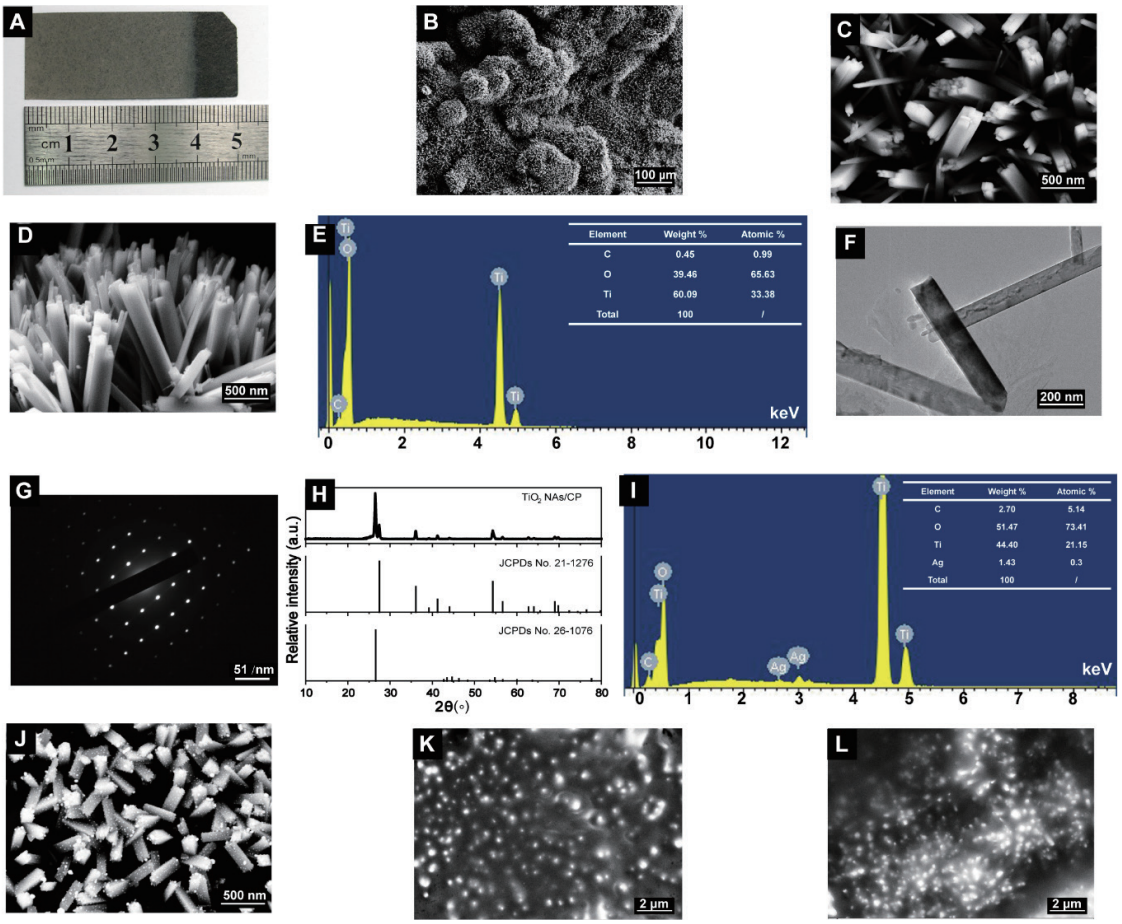

Fig. 2. (Color online) (A) Photograph of TiO2 NAs/CP. SEM images of (B and C) top and (D) bird's eye views of TiO_2 NAs/CP. (E) EDS of TiO_2 NAs/CP. (F) TEM image and (G) SAED pattern of TiO_2 NRs. (H) XRD spectrum of TiO2 NAs/CP, standard card of rutile TiO_2 (JCPDs Card No. 21-1276) and standard card of carbon (JCPDs Card No. 26-1076). (I) EDS of Ag NPs-TiO_2 NAs/CP. SEM images of (J) Ag NPs-TiO_2, (K) GOx/TiO_2, and (L) GOx/Ag NPs-TiO_2 NAs/CP electrodes.

Then, the Ag NPs were deposited on the surface of TiO_2 NAs to fabricate the Ag NPs-TiO_2 NAs/CP electrode and investigated by SEM and EDS. As shown in Fig. 2(J), the Ag NPs were uniformly deposited on the surface of TiO_2 NAs with an average diameter of approximately 10 nm. Moreover, a small amount of 30–40 nm Ag NPs aggregated on the surface of TiO_2 NAs with little effect on the overall catalytic performance. Figure 2(I) shows the EDS of the Ag NPs-TiO_2 NAs/CP electrode. Compared with the TiO_2 NAs/CP [Fig. 2(E)], the Ag NPs-TiO_2 NAs/CP electrode was composed of four elements, C, O, Ti, and Ag. Ag was from the Ag NPs, indicating that the Ag NPs were deposited on the TiO_2 NAs/CP electrode.

Thereafter, the GOx enzymes were immobilized on the surfaces of the TiO_2 NAs/CP and Ag NPs-TiO_2 NAs/CP electrodes via the crosslinking of GOx and BSA. Compared with the Ag NPs-TiO_2 NAs/CP electrode [Fig. 2(J)], owing to GOx immobilization, a layer of uniform covering was observed on the surfaces of GOx/TiO_2 NAs/CP [Fig. 2(K)] and GOx/Ag NPs-TiO_2 NAs/CP

[Fig. 2(L)], indicating that the GOx enzymes were fixed on the surfaces of the TiO_2 NAs and Ag NPs-TiO_2 NAs. In addition, owing to the thick BSA and GOx layer, the Ag NPs could not be clearly observed in Fig. 2(L). These results all demonstrated that large amounts of GOx enzymes were fixed on the electrode, suggesting the successful fabrication of the GOx/Ag NPs-TiO_2 NAs/CP electrode.

3.2 Electrocatalytic activity of Ag NPs-TiO2 NAs/CP electrode for H2O2

Cyclic voltammetry was carried out to investigate the electrocatalytic activity of the Ag NPs-TiO_2 NAs/CP electrode for H_2O_2. Figure 3 shows the cyclic voltammetric curves of the CP, TiO_2 NAs/CP, and Ag NPs-TiO_2 NAs/CP electrodes in H_2O_2 solutions of various concentrations (0, 0.5, and 1.0 mM) with a scanning potential range of −1.0–1.0 V and a scanning rate of 50 mVs^{-1}. Figure 3(A) shows that there was no reduction peak in the whole range of the CP electrode. However, the clear reduction of the peak near the potential of −0.6 V with the increase in H_2O_2 concentration observed for the TiO_2 NAs/CP [Fig. 3(B)] and Ag NPs-TiO_2 NAs/CP [Fig. 3(C)] electrodes was attributed to the H_2O_2 reduction on the electrode surface. Therefore, we selected

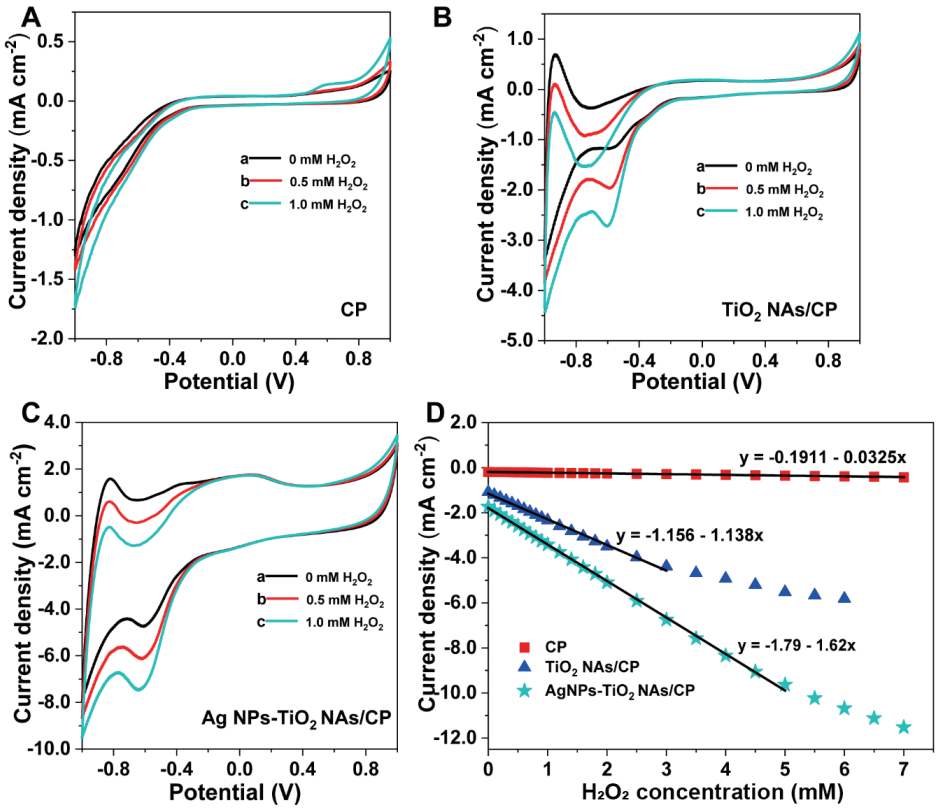

Fig. 3. (Color online) Electrocatalytic activities of different electrode materials for H_2O_2. Cyclic voltammetric curves for (A) CP, (B) TiO_2 NAs/CP, and (C) Ag NPs-TiO2 NAs/CP electrodes. (D) Linear relationships between H_2O_2 concentration and current density for the three electrode materials.

−0.6 V as the working potential for responding to H_2O_2. The current reduction increased with increasing H_2O_2 concentration for all the three electrode materials.

Figure 3(D) shows the linear relationships between the H_2O_2 concentration and the curve of the response current for the three electrode materials. It can be seen that the CP, TiO_2 NAs/CP, and Ag NPs-TiO_2 NAs/CP electrodes respond to H_2O_2 in the ranges of 0–7, 0–3, and 0–5 mM, respectively. Moreover, the sensitivity to the H_2O_2 concentration for the Ag NPs-TiO_2 NAs/CP electrode was estimated to be 1.62 mA $mM^{-1}cm^{-2}$, which was 50-fold that for the CP electrode (0.0325 mA $mM^{-1}cm^{-2}$) and 1.42-fold that for the TiO_2 NAs/CP (1.138 mA $mM^{-1}cm^{-2}$). Therefore, these results demonstrated that the electrocatalytic activity for H_2O_2 for the Ag NPs-TiO_2/CP electrode is better than those for the CP and TiO_2/CP electrodes.

3.3 Performance of GOx/Ag NPs-TiO2 NAs/CP electrode for glucose detection

Figure 4 shows the cyclic voltammetric curves of the GOx/CP, GOx/TiO_2 NAs/CP, and GOx/Ag NPs-TiO_2 NAs/CP biosensors in PBS solution without glucose (curve a), with 0.5 mM glucose (curve b), and with 1.0 mM glucose (curve c). It can be seen that the reduction peak of the cyclic voltammetry curve for the GOx/CP biosensor at −0.5 V and those for the GOx/TiO_2 NAs/CP and GOx/Ag NPs-TiO_2 NAs/CP biosensors at −0.6 V decrease with increasing glucose concentration, indicating that the GOx enzymes can promote the decomposition of glucose for the three electrodes. Therefore, we selected −0.5 V as the working potential measuring the time current curve for GOx/CP biosensors and −0.6 V as that for both the GOx/TiO_2 NAs/CP and GOx/Ag NPs-TiO_2 NAs/CP biosensors. Figures 4(D)–(F) show the time current curves responding to the addition of different concentrations of glucose at the optimal constant potential for the GOx/CP, GOx/TiO_2 NAs/CP, and GOx/Ag NPs-TiO_2 NAs/CP biosensors, respectively. In this assay, glucose solution was added for detection every 50 s, and the glucose concentration increased by 0.05 mM each time from the 100th s. Then, the glucose concentration increased by 0.1 mM for each addition from the 400th s until the end of the test. The resulting biosensors indicate rapid and sensitive responses to the addition of glucose, which reached the steady-state current within 5 s. The results might be attributed to the high porous structure of the GOx-Ag-TiO_2/CP biosensors, which provided a large surface for the interaction of GOx with glucose.

As exhibited in Fig. 4(G), the sensitivity to glucose for the GOx/Ag NPs-TiO_2 NAs/CP biosensor was estimated to be 0.182 mA $mM^{-1}cm^{-2}$, which was 6.6-fold that for the GOx/CP biosensor (0.0276 mA $mM^{-1}cm^{-2}$) and 1.4-fold that for the GOx/TiO_2 NAs/CP biosensor (0.13 mA $mM^{-1}cm^{-2}$). Therefore, compared with the GOx/CP and GOx/TiO_2 NAs/CP biosensors, the GOx/Ag NPs-TiO_2 NAs/CP biosensor exhibited much better electrocatalytic performance for glucose. The relationship between the glucose concentration and the sensitivity to glucose is linear with the correlation coefficient R^2 of 0.9996 in the range of 0–0.9 mM, and the detection limit was estimated to be 1.6 μM. The sensitivity for the GOx/Ag NPs-TiO_2 NAs/CP biosensor is almost equivalent to those for other sensors at micromolar levels.[16,17]

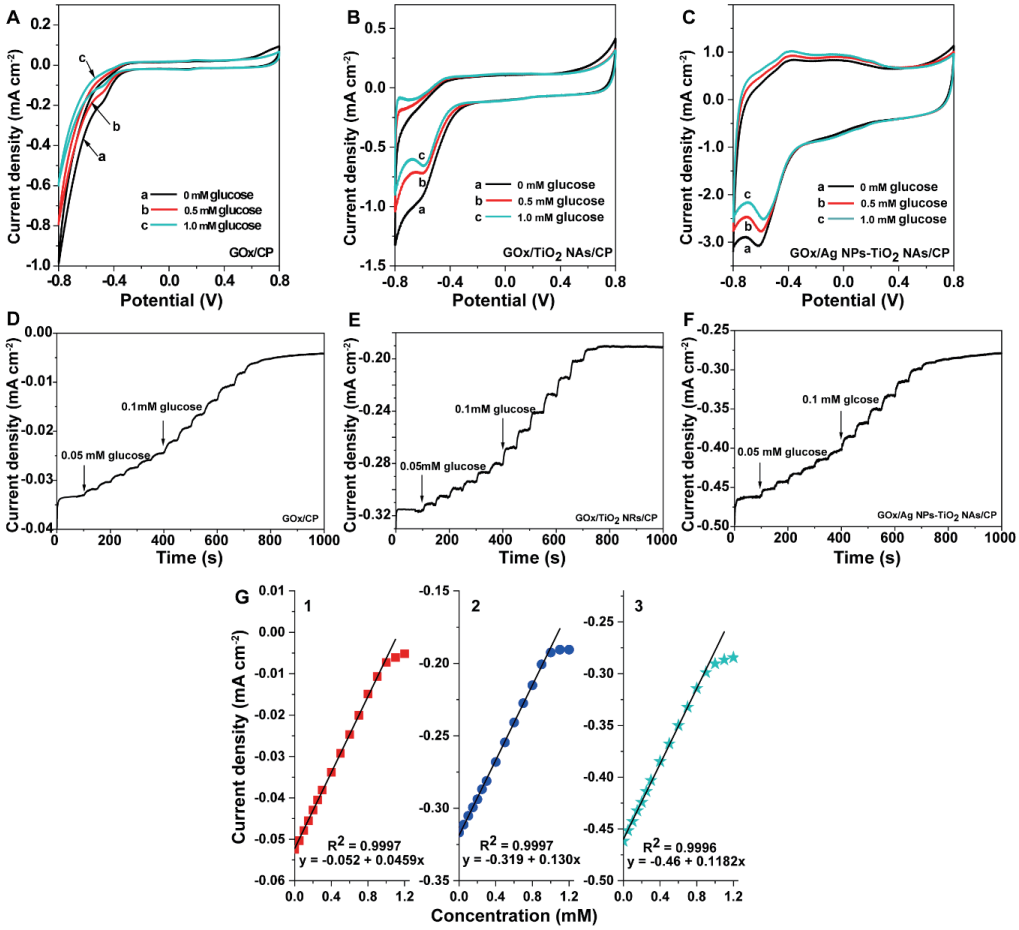

Fig. 4. (Color online) Electrocatalytic activities of different electrode materials for glucose detection. Cyclic voltammetric curves of (A) CP, (B) TiO_2 NAs/CP, and (C) Ag NPs-TiO_2 NAs/CP electrodes. Time current curves responding to the different concentrations of glucose for the (D) CP, (E) TiO2 NAs/CP, and (F) Ag NPs-TiO_2 NAs/CP electrodes. (G) Linear relationships between the glucose concentration and the current density for the (1) CP, (2) TiO_2 NAs/CP, and (3) Ag NPs-TiO_2 NAs/CP electrodes.

4. Conclusion

TiO_2 NAs were hydrothermally synthesized on a CP substrate, and then Ag NPs were deposited on the surface of TiO_2 NAs (termed Ag NPs-TiO_2 NAs/CP electrode). The sensitivity to H_2O_2 for the Ag NPs-TiO_2 NAs/CP electrode was estimated to be 1.62 mA $mM^{-1}cm^{-2}$, which was 50-fold that for the CP electrode and 1.42-fold that for the TiO_2 NAs/CP electrode, indicating that the Ag NPs enhance the electrocatalytic activity and analysis ability of the electrode for H_2O_2. GOx was immobilized on the electrode surface to prepare the GOx electrode via the crosslinking method. In an *in vitro* test, this sensor showed a linear response, a high sensitivity of 0.182 mA $mM^{-1}cm^{-2}$, and a detection limit of 1.6 μM after optimizing experimental parameters. In the near future, a biological interference study of this sensor should be carried out to test for the detection of glucose in real blood samples.

Acknowledgments

This work was supported by the Natural Science Foundation of China (81901798 and 32201168), the Natural Science Fund for Colleges and Universities in Jiangsu Province (19KJB310025), the Science and Technology Development Program of Xuzhou (KC21066 and KC22253), the Startup Fund for Youth Talent in Xuzhou Medical University (D2020052), and the Scientific Research Project of the Health Commission of Jiangsu Province (Z2022007).

References

1 J. A. Al-Lawati: Diabetes Mellitus: Oman. Med. J. **32** (2017) 177. https://doi.org/10.5001/omj.2017.34
2 N. Mano: Bioelectrochemistry **128** (2019) 218. https://doi.org/10.1016/j.bioelechem.2019.04.015
3 P. Mandpe, B. Prabhakar, H. Gupta, and P. Shende: Sensor Rev. **40** (2020) 497. https://doi.org/10.1108/Sr-01-2019-0017
4 S. A. Pullano, M. Greco, M. G. Bianco, D. Foti, A. Brunetti, and A. S. Fiorillo: Theranostics **12** (2022) 493. https://doi.org/10.7150/thno.64035
5 Y. Zhang, S. Li, H. Y. Liu, F. Shi, J. Li, X. Y. Hu, and Z. J. Yang: Analyst **147** (2022) 4049. https://doi.org/10.1039/d2an01003h
6 V. Scognamiglio and F. Arduini: TrAC Trends Anal. Chem. **120** (2019) 115642. https://doi.org/10.1016/j.trac.2019.115642
7 H. Farhat, J. Celier, C. Forano, and C. Mousty: Electrochim. Acta **376** (2021) 138050. https://doi.org/10.1016/j.electacta.2021.138050
8 M. Gijare, S. Chaudhari, S. Ekar, S. F. Shaikh, R. S. Mane, B. Pandit, M. U. H. Siddiqui, and A. Garje: Electronics **12** (2023) 294. https://doi.org/10.3390/electronics12020294
9 W. T. Chiu, T. F. M. Chang, M. Sone, A. Tixier-Mita, and H. Toshiyoshi: Talanta **212** (2020) 120780. https://doi.org/10.1016/j.talanta.2020.120780
10 W. Wang, Y. B. Xie, C. Xia, H. X. Du, and F. Tian: Microchim. Acta **181** (2014) 1325. https://doi.org/10.1007/s00604-014-1258-x
11 Z. Xie, F. T. Zhao, S. M. Zou, F. Zhu, Z. J. Zhang, and W. P. Wang: J. Alloy. Compd. **861** (2021) 157999. https://doi.org/10.1016/j.jallcom.2020.157999
12 A. X. Jiao, Q. Q. Cui, S. Li, H. S. Li, L. L. Xu, Y. Tian, H. Ma, M. Y. Zhang, X. D. Liu, and M. Chen: Sens. Actuators, B **350** (2022) 130848. https://doi.org/10.1016/j.snb.2021.130848
13 S. L. Wu, Z. Y. Weng, X. M. Liu, K. W. K. Yeung, and P. K. Chu: Adv. Funct. Mater. **24** (2014) 5464. https://doi.org/10.1002/adfm.201400706
14 W. Smith, S. Mao, G.H. Lu, A. Catlett, J. H. Chen, and Y. P. Zhao: Chem. Phys. Lett. **485** (2010) 171. https://doi.org/10.1016/j.cplett.2009.12.041
15 A. John, L. Benny, A.R. Cherian, S. Y. Narahari, A. Varghese, and G. Hegde: J. Nanostruct. Chem. **11** (2021) 1. https://doi.org/10.1007/s40097-020-00372-8
16 Y. Wang, H. J. Guo, M. Yuan, J. B. Yu, Z. P. Wang, and X. P. Chen: Talanta **257** (2023) 124362. https://doi.org/10.1016/j.talanta.2023.124362
17 K. Puttananjegowda, A. Takshi, and S. Thomas: Biosens. Bioelectron **186** (2021) 113285. https://doi.org/10.1016/j.talanta.2023.124362